ELSEVIER

Precipitation in AISI 316L(N) during creep tests at 550 and 600 °C up to 10 years

A.F. Padilha [a], D.M. Escriba [a], E. Materna-Morris [b,*], M. Rieth [b], M. Klimenkov [b]

[a] *University of S. Paulo, Department of Metallurgical and Materials Engineering, Av. Prof. Mello Moraes 2463,
CEP 05508-900, S. Paulo, Brazil*
[b] *Forschungszentrum Karlsruhe, Institut für Materialforschung I, P.O. Box 3640, 76021 Karlsruhe, Germany*

Abstract

The precipitation behaviour in the gauge lengths and in the heads of initially solution annealed type 316L(N) austenitic stainless steel specimens tested in creep at 550 and 600 °C for periods of up to 85 000 h has been studied using several metallographic techniques. Three phases were detected: $M_{23}C_6$, Laves, and sigma phase. The volume fraction of the precipitated sigma phase was significantly higher than that of carbides and the Laves phase. $M_{23}C_6$ carbide precipitation occurred very rapidly and was followed by the sigma and Laves phases formation in the delta ferrite islands. Sigma and Laves phases precipitated at grain boundaries after longer times. Two different mechanisms of sigma phase precipitation have been proposed, one for delta ferrite decomposition and another for grain boundary precipitation. Small quantities of the Laves phase were detected in delta ferrite, at grain boundaries and inside the grains.
© 2007 Elsevier B.V. All rights reserved.

PACS: 61.82.Bg; 68.37.Lp; 68.37.Hk

1. Introduction

The sigma phase (σ) is probably the most studied intermetallic phase in stainless steels. Already in 1907, even before the discovery of stainless steels, Treitschke and Tammann [1] studied the Fe–Cr system and proposed the existence of an intermetallic compound containing 30–50 wt% of chromium. In 1927, Bain and Griffiths [2] studied the Fe–Cr–Ni system and observed a hard and fragile phase, which they called constituent B, denoting 'brittle'. In 1936, Jett and Foote [3] called it sigma phase and in 1951, Bergmann and Shoemaker [4] determined through crystallography its structure in the Fe–Cr system.

Precipitation of the sigma phase in stainless steels may occur in the austenitic, ferritic, and ferritic–austenitic with a duplex structure type. The precipitation of the sigma phase does not only cause losses of ductility and toughness of the steel, but also reduces its corrosion resistance by removing chromium and molybdenum from the austenitic matrix.

In the austenitic stainless steels [5–11], sigma phase precipitation generally requires hundreds or

* Corresponding author. Tel.: +49 7247 82 2162; fax: +49 7247 82 4567.

E-mail address: materna-morris@imf.fzk.de (E. Materna-Morris).

even thousands of hours and the precipitated volumetric fraction generally is smaller than 5%. Precipitation may be represented by a common precipitation reaction: $\gamma \rightarrow \gamma* + \sigma$, where $\gamma*$ is a chromium- and molybdenum-depleted austenite compared to the original austenite. Precipitation occurs predominantly at grain boundaries, especially at triple points. In the case of duplex stainless steels [12,13], precipitation may be completed within a few hours and consumes nearly all ferrite of the microstructure. Precipitation in this case can be represented by a eutectoid type reaction: $\alpha \rightarrow \gamma** + \sigma$, where $\gamma**$ is known as *new austenite*. Precipitation starts at the α/γ interface and moves into the ferrite grain.

Austenitic stainless steels of the type AISI 316L are widely used in components designed for high-temperature applications. It is also used or envisaged for use in both conventional and nuclear plant constructions as well as in the international nuclear fusion project. Long-term exposure of this steel to high-temperatures is known [5–11] to cause the precipitation of several carbides, such as $M_{23}C_6$, and M_6C and intermetallic phases, such as sigma (σ), chi (χ) and Laves phases. Steel charges with higher $(Cr + Mo)/Ni$ ratios are more prone to intermetallic phases precipitation. On the other hand, C and N in solid solution prevent the formation of the sigma phase due to its inability to dissolve these elements. During solidification or welding of austenitic stainless steels, the formation of delta ferrite may occur, which may be difficult to eliminate completely during thermo-mechanical processing and present before the solution-annealing heat treatment. It may even survive it. Delta ferrite reduces the tendency of austenitic stainless steels to hot cracking during welding. If the austenitic stainless steel contains delta ferrite, it may be even more susceptible to sigma phase precipitation [8]. Cold work prior to ageing accelerates the sigma phase formation [6]. Simultaneous creep straining also increases the precipitation rate in the steel type AISI 316 [14–18]. On the other hand, most of the work published on sigma phase precipitation in type 316 stainless steel was performed using delta ferrite-free

charges. Besides, the exposure time rarely exceeded 10 000 h.

The principal aim of the present work was to obtain detailed information on the nature, extent, morphology, and distribution of sigma phase precipitation in head and gauge length of AISI 316L(N) austenitic stainless steel specimens during long-term creep tests at 550 and 600 °C. A steel charge containing residual delta ferrite stringers was selected for this investigation.

2. Experimental procedures

The material investigated (for chemical composition see Table 1) was a nitrogen-alloyed, low-carbon grade of the type 316L(N) austenitic stainless steel, supplied as a 40 mm thick hot-rolled plate that had been subjected to final solution annealing at 1100 °C for 30 min, followed by water quenching, which produced a grain size of about 120 μm. Creep specimens were machined from the centre of the plate, transverse to rolling direction. Two different sizes of round cross-section creep specimens were used (see Table 2). The increased length of 200 mm ensured that the measurement of the creep behavior was much more accurate than for standard specimens. The test temperatures (550 and 600 °C) were controlled by means of three Pt–PtRh thermocouples and kept constant at ±2 K. The creep specimens produced are shown in Table 2. Specimen details, testing techniques, and creep results were described previously [19].

Longitudinal and transverse sections of the gauge and head portions of the specimens were examined before and after creep tests using optical microscopy (OM), scanning electron microscopy (SEM), and transmission electron microscopy (TEM). For optical metallography, specimens were etched in either V2A-etchant, 5% HCl in ethanol or Aqua Regia [20,21]. For SEM investigations by employing a Philips XL30 microscope, specimens were etched in V2A-etchant. A large number of precipitated particles was analysed using a combination of SEM and energy-dispersive X-ray spectroscopy. TEM samples were prepared by electro-polishing the discs in

Table 1
The chemical composition of the AISI 316L(N) austenitic stainless steel investigated (wt%)

C	Si	Mn	P	S	Cr	Ni	Mo	Cu	N	Al	B
0.02	0.32	1.80	0.02	0.006	17.34	12.50	2.40	0.12	0.08	0.018	0.0014

Table 2
Creep test specimens investigated in this work

Temperature (°C)	Stress (MPa)	Time (h)	Initial strain (%)	Specimen dimensions diameter × length (mm)
550	150	6100	7.5	8 × 200
550	210	60 000	4.8	8 × 200
550	135	70 000	0.34	8 × 200
550	180	85 000	2.85	8 × 200
600	280	83 (rupture)	10.0	5 × 30
600	260	164 (rupture)	8.8	5 × 30
600	200	5481 (rupture)	3.7	5 × 30
600	170	7500	5.0	8 × 200
600	120	41 015	0.2	8 × 200
600	70	85 000	0.005	8 × 200

a TENUPOL device using $H_2SO_4 + 80\%\ CH_3OH$ as electrolyte. The TEM investigations were performed at an accelerating voltage of 200 kV using a FEI Tecnai 20 FEG microscope equipped with an electron energy loss spectrometer (EELS) and a Gatan image filter (GIF). for EFTEM (energy filtered TEM) measurements. The EELS spectra were measured with the focused probe in the STEM regime using a high-angle annular dark field (HAADF) detector with a 3 mm window.

3. Results and discussion

The micrographs shown in Figs. 1 and 2 exhibit the steel microstructure in the solution-annealed condition, revealing the presence of recrystallised grains, annealing twins, and delta ferrite islands.
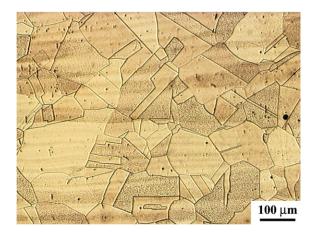

Fig. 1. Optical micrograph of solution-annealed 316L(N) stainless steel, revealing the presence of recrystallised grains and annealing twins. Etching: V2A-etchant.
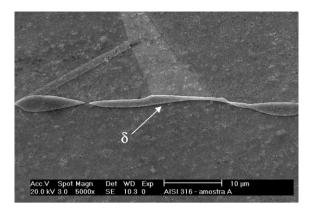

Fig. 2. Scanning electron micrograph (secondary electrons) of solution-annealed 316L(N) stainless steel, showing details of the delta (δ) ferrite phase. Etching: V2A-etchant.

Stainless steels can solidify by several mechanisms or modes: ferritic or mode A $(L \rightarrow L + \delta \rightarrow \delta)$; ferritic–austenitic or mode B $(L \rightarrow L + \delta \rightarrow L + \delta + \gamma \rightarrow \gamma + \delta)$; austenitic–ferritic or mode C $(L \rightarrow L + \gamma \rightarrow L + \gamma + \delta \rightarrow \gamma + \delta)$ and austenitic or mode D $(L\ (liquid) \rightarrow L + \gamma \rightarrow \gamma)$. The prediction of their solidification mode and sequence may be successfully evaluated in advance using chromium and nickel equivalence ratios [22]. Delta ferrite was formed during solidification and not completely dissolved during thermo-mechanical processing and subsequent solution annealing. The annealing twins are typical of low-stacking-fault-energy FCC metals and solid solutions [23].

The sequence of precipitation and resolution or dissolution (in the case of $M_{23}C_6$) of the various phases are summarized in Fig. 3.

The $M_{23}C_6$ (M = Cr, Fe, Mo, Ni) carbide is normally the first phase to form in austenitic stainless steels. Precipitates of this phase were detected at grain boundaries in the gauge length and head of creep-tested specimens after 83 h. The solubility of carbon in 316 steel [24] at 600 °C is about 4 ppm only. Carbide formation is rapid due to the availability of chromium and the fast diffusion of interstitial carbon atoms. After long-term creep tests and intermetallic phases precipitation, grain-boundary carbides were not found. The intermetallic phases precipitation can lower the Mo and Cr contents of the matrix, increasing the carbon solubility and leading to $M_{23}C_6$ dissolution [5,6].

The occurrence of the sigma phase was also detected in the ferrite islands in the gauge length and head of creep-tested specimens after 83 h. Sigma phase precipitation in austenite was detected

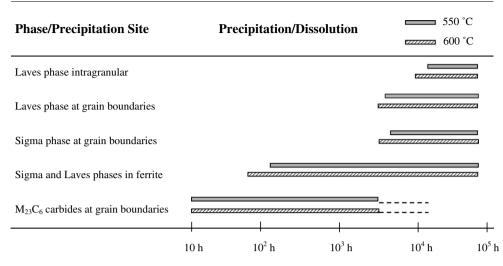| Phase/Precipitation Site | Precipitation/Dissolution | 550 ˚C |
| | | 600 ˚C |

Fig. 3. Schematic diagram of phase reactions during ageing of AISI 316L(N) at 550 and 600 °C.

only after 5481 h of creep test. The sigma phase particles formed predominantly at the grain boundaries, often at triple points. As pointed out by Barcik [8], the rate of sigma phase precipitation from ferrite is about 100 times more rapid than the rate of sigma phase precipitation directly from austenite. Concurrent creep straining did not increase significantly the rate of sigma phase precipitation. Figs. 4 and 5 show sigma phase formation in delta ferrite and at grain boundaries after 85 000 h, respectively. Table 2 shows the contents (in wt%) of the principal metallic elements in austenite, delta ferrite, sigma phase, and Laves phase as determined by energy-dispersive X-ray spectroscopy.

As mentioned above, sigma phase precipitation in austenite has a very slow kinetics. There are at least three reasons for the slow kinetics: (a) carbon and nitrogen are insoluble in the sigma phase; as a consequence, the sigma phase normally appears only after carbide, nitride or carbonitride precipitation has taken place and the matrix is depleted in carbon and nitrogen; (b) its nucleation is difficult on account of its crystal structure being complex and very different from the parent austenite; and (c) it is very rich in substitutional elements, thus requiring extended diffusion times [10,11]. On the other hand, sigma formation via a cooperative eutectoid-type reaction is easier and quicker. Delta ferrite, enriched in Cr and Mo (see Table 3), exhibits a more pronounced tendency to sigma phase
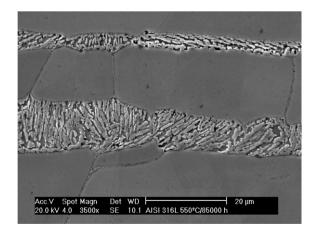

Fig. 4. Sigma (σ) phase formation from delta ferrite islands after 85 000 h creep test at 550 °C. Etching: V2A-Beize. SEM. SE.
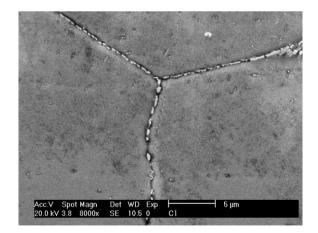

Fig. 5. Sigma (σ) phase precipitation at austenite grain boundary and triple points after 85 000 h creep test at 550 °C. Etching: 5% HCl in ethanol. SEM. SE.

Table 3
Contents of principal metallic elements in austenite, delta ferrite, sigma phase, and Laves phase as determined by energy-dispersive X-ray spectroscopy (wt%)

Phase	Si	Mo	Cr	Mn	Fe	Ni
Matrix (γ), initial	0.54 ± 0.2	2.6 ± 0.1	17.4 ± 0.2	2.0 ± 0.1	64.9 ± 0.3	12.4 ± 0.1
Delta (δ) ferrite, initial	0.51 ± 0.5	4.7 ± 0.1	23.9 ± 0.2	1.51 ± 0.04	63.2 ± 0.2	6.11 ± 0.02
Sigma (σ) phase in δ-ferrite	0.42 ± 0.2	5.9 ± 0.3	39 ± 2	1.3 ± 0.1	47 ± 2	5.9 ± 0.6
Sigma (σ) phase at triple point	0.47 ± 0.4	4.3 ± 0.3	25 ± 1	1.51 ± 0.03	58 ± 2	10.6 ± 0.2
Laves (η) phase in δ-ferrite	2.5 ± 0.1	21.9 ± 0.8	18 ± 2	1.1 ± 0.2	52 ± 2	4 ± 1

formation than the austenite. Moreover, the rate of Cr and Mo diffusion in ferrite is almost 100 times higher than in austenite. A comparison of the present data with previously published results [5,6] from the precipitation behavior of type AISI 316L steel suggests that the effect of delta ferrite on the sigma phase precipitation kinetics is stronger than the effects of minor compositional changes. Fig. 6 shows a schematic presentation of sigma phase formation [25,26] in AISI 316L(N) at 550 and 600°C. Two reaction types are presented in Fig. 6: (a) an eutectoid reaction in delta ferrite ($\delta \rightarrow \sigma + \gamma$); and (b) a common solid-state precipitation reaction at grain boundaries ($\gamma \rightarrow \sigma + \gamma$).

The Laves phase (η) is frequently found in AISI 316, 316L, and 316L(N) austenitic stainless steels [5–11,15–18]. According to Minami et al. [7], precipitation of the Laves phase Fe_2Mo at 600 °C in an AISI 316H austenitic stainless steel occurred before precipitation of the sigma phase. At 600 °C, where the chi (χ) phase normally is absent, its formation interacts in a competitive way with that of the sigma phase. According to Sourmail [9], the presence of delta ferrite delays the Laves phase formation because it enhances that of the sigma phase. In this work, the Laves phase (η) was detected in delta ferrite (see Fig. 7) and at grain boundaries together with the sigma phase. After longer exposure times, it also precipitated intra-granularly (see Figs. 7–9). The chi phase was not detected in this work. It is mainly found [5–11] in type 316 steel above 750 °C.
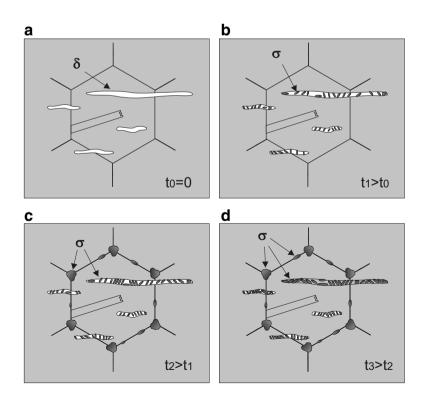

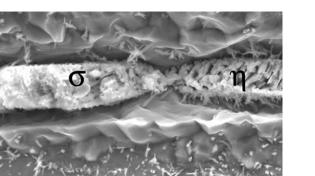Fig. 6. Schematic presentation of sigma phase formation [25,26] in AISI 316L(N) at 550 and 600 °C.

Fig. 7. Micrographs of the gauge length of the tested specimen (600 °C/70 MPa/85 000 h), showing precipitation of the sigma and Laves phases in delta ferrite, and intra-granular precipitation of the Laves phase. Deep etching with V2A-etchant. SEM. SE.

Fig. 8. Micrograph showing sigma phase precipitation at grain boundaries and intra-granular precipitation of the Laves phase after 85 000 h creep test. Deep etching with V2A-etchant. SEM. SE.

Fig. 9 shows the results of the chemical and structural microanalysis of a Laves phase particle precipitated inside the grain. Compared to the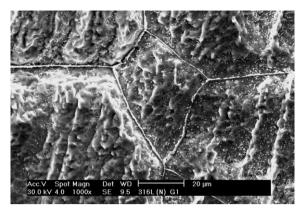 austenitic matrix, the particle shows Mo and Si enrichment and Fe and Ni depletion. The chemical composition of this particle agrees fairly well with that of the Laves phase found in delta ferrite (see Table 3).

Finally, it is interesting to compare the microstructural stability of the steel studied in the present
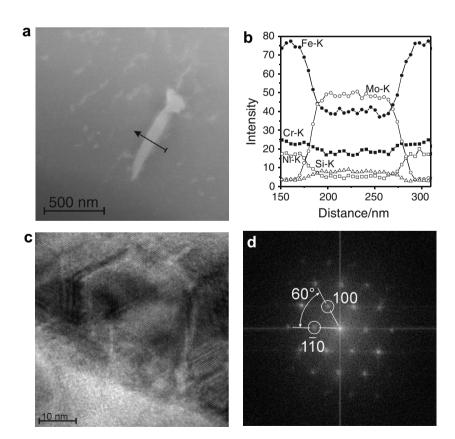

Fig. 9. TEM analysis of the Laves phase: (a) bright-field image; (b) Fe, Cr, Ni, Mo, and Si profiles along the arrow in (a); (c) high-resolution image of the Laves phase; (d) zone axis [0 0 1], hexagonal structure with $a = 0.4745$ nm and $c = 0.7734$ nm.

work with the DIN W. Nr. 1.4970 (15%Cr–15%Ni–1.2%Mo–Ti) steel. The fully austenitic stainless steel 1.4970 was originally developed for use as cladding material in the German sodium-cooled fast breeder nuclear reactor SNR 300 [27,28]. Delta ferrite, strain induced martensites and intermetallic phases such as sigma, chi and Laves phases can be present in the microstructure of the most unstabilized and stabilized austenitic stainless steels such as AISI 316, AISI 316L, AISI 316L(N), AISI 321 and AISI 347 [5–11]. On the other hand, the steel 1.4970 is not susceptible to the formation of delta ferrite, martensite and intermetallic phases, due to its relatively low-Cr/Ni ratio and well adjusted molybdenum and titanium contents [27,28].

4. Conclusions

(1) Three phases were detected: $M_{23}C_6$, sigma, and Laves phases. The volume fraction of the precipitated sigma phase was significantly higher than those of carbides and the Laves phase.

(2) Precipitation during creep tests commenced with the rapid formation of $M_{23}C_6$ at grain boundaries.

(3) Carbide precipitation was followed by sigma phase formation in the delta ferrite islands via the eutectoid reaction $\delta \rightarrow \sigma + \gamma$. The sigma phase precipitated at grain boundaries after longer times.

(4) The effect of delta ferrite on the sigma phase precipitation kinetics is stronger than the effects of minor compositional changes.

(5) Concurrent creep straining did not increase significantly the rate of sigma phase precipitation.

(6) The Laves phase precipitated concurrently with the sigma phase in delta ferrite and at grain boundaries. After longer exposure times, the phase also precipitated intra-granularly.

(7) After long-term exposure, grain-boundary carbides were not found. Nor was the chi (χ) phase detected in this work.

Acknowledgements

References

[1] W. Treitschke, G. Tammann, Z. Anorg. Chem. 55 (1907) 402.
[2] E.C. Bain, W.E. Griffiths, Trans. AIME 75 (1927) 166.
[3] E.R. Jett, F. Foote, Met. Alloys 7 (1936) 207.
[4] B.G. Bergmann, D.P. Shoemaker, J. Chem. Phys. 19 (1951) 515.
[5] H. Wiegand, M. Doruk, Arch. Eisenhüttenwes. 8 (1962) 559.
[6] B. Weiss, R. Stickler, Metall. Trans. 3 (1972) 851.
[7] M. Minami, H. Kimura, Y. Ihara, Mater. Sci. Technol. 2 (1986) 795.
[8] J. Barcik, Mater. Sci. Technol. 4 (1988) 5.
[9] T. Sourmail, Mater. Sci. Technol. 17 (2001) 1.
[10] A.F. Padilha, P.R. Rios, ISIJ Int. (Japan) 42 (2002) 325.
[11] P.R. Rios, A.F. Padilha, in: K.H. Buschow et al. (Eds.), Encyclopedia of Materials: Science and Technology Updates, Elsevier, Amsterdam, 2005.
[12] A.F. Padilha, F.C. Pimenta Jr., W. Reick, Z. Metallkd. 92 (2001) 351.
[13] M. Pohl, O. Storz, Z. Metallkd. 95 (2004) 631.
[14] D.G. Morris, D.R. Harries, Met. Sci. 12 (1978) 542.
[15] G. Sasikala, M.D. Mathew, K. Bhanu Sankara Rao, S.L. Mannan, J. Nucl. Mater. 273 (1999) 257.
[16] G. Sasikala, S.K. Ray, S.L. Mannan, Mater. Sci. Eng. A 359 (2003) 86.
[17] G. Sasikala, S.K. Ray, S.L. Mannan, Acta Mater. 52 (2004) 5677.
[18] T. Nakazawa, H. Kimura, K. Kimura, H. Kaguchi, J. Mater. Process. Technol. 143–144 (2003) 905.
[19] M. Rieth, A. Falkenstein, P. Graf, S. Reger, U. Jäntsch, M. Klimiankou, E. Materna-Morris, H. Zimmermann, Forschungszentrum Karlsruhe, Report FZKA-7065, November 2004.
[20] G. Petzow, Metallographic etching, American Society for Metals (ASM), Metals Park, Ohio, USA, 1978.
[21] H. Schumann, H. OettelMetallografie, vol. 14, Auflage, Wiley-VCH Verlag, Weinheim, 2005.
[22] G.K. Allan, Ironmak. Steelmak. 22 (1995) 465.
[23] A.F. Padilha, R.L. Plaut, P.R. Rios, ISIJ Int. (Japan) 43 (2003) 135.
[24] M. Deighton, J. Iron Steel Inst. 208 (1970) 1012.
[25] D.M. Escriba Villanueva, PhD thesis, University of S. Paulo, Brazil, 2005.
[26] D.M.E. Villanueva, F.C.P. Junior, R.L. Plaut, A.F. Padilha, Mater. Sci. Technol. (London) 22 (2006) 1098.
[27] A.F. Padilha, G. Schanz, K. Anderko, J. Nucl. Mater. 105 (1982) 77.
[28] M. Terada, M. Saiki, I. Costa, A.F. Padilha, J. Nucl. Mater. 358 (2006) 40.